IEEE Access
Multidisciplinary | Rapid Review | Open Access Journal

Received November 9, 2021, accepted November 20, 2021, date of publication November 23, 2021,
date of current version December 2, 2021.

Digital Object Identifier 10.1109/ACCESS.2021.3130205

Applying Characteristic Mode Analysis to Systematically Design of 5G Logarithmic Spiral MIMO Patch Antenna

AHMED ABDELAZIZ[1], HESHAM A. MOHAMED[2], (Senior Member, IEEE), AND EHAB K. I. HAMAD[3], (Member, IEEE)

[1]Department of Electronics and Communications, Luxor Higher Institute of Engineering and Technology, Luxor 85834, Egypt
[2]Department of Microstrip Circuits, Electronics Research Institute, Dokky, Giza 11843, Egypt
[3]Department of Electrical Engineering, Faculty of Engineering, Aswan University, Aswan 81542, Egypt

Corresponding author: Ahmed Abdelaziz (d20190014@aswu.edu.eg)

ABSTRACT The Theory of Characteristic Modes (TCM) provides a natural and systematic approach for designing Multiple-Input Multiple-Output (MIMO) antennas with high efficiency and uncorrelated antenna patterns. Recent progress in the growing field of MIMO antenna design, supported by TCM, is examined in this study. The challenge of designing MIMO antennas for 5G wireless communications is particularly highlighted. The results demonstrate that the characteristic modes play a key role in establishing the optimal positioning of antennas for optimal efficiency. Therefore, in this article, this theory is applied to a novel design of a logarithmic spiral patch antenna (LSPA) that is used to obtain a circular polarization with good performance more easily than traditional shapes. The systematic design process starts by designing a single element with one logarithmic spiral arm and passing through adding another arm of this single element, also passing through a two-element array antenna, and ending in four configurations of two-port MIMO and selecting the configuration with the best performance. The best configuration of the proposed MIMO provides a wide -10 dB measured impedance ranging from 27.3 GHz to 30.2 GHz, covering the whole frequency band allocated for 5G communication systems with acceptable performance as large bandwidth, high gain, high isolation, low envelope correlation coefficient, and low channel capacity loss. The isolation achieved for the operating bandwidth is better than −36 dB, demonstrating low mutual coupling. Moreover, the peak gain and total efficiency obtained are 9.9 dBi and 94%, respectively, over the whole operating bandwidth. The proposed design is designed, analyzed, and simulated in the 3D electromagnetic full-wave software, Computer Simulation Technology (CST). The design was fabricated using the photo-lithographic method and measured using the R&SZNA67 vector network analyzer. The prototype achieved is extremely similar to the expected performance and consequently proves that the offered characteristics mode analysis method is applicable.

INDEX TERMS 5G, characteristic mode analysis (CMA), circularly polarized (CP), isolation enhancement, logarithmic spiral patch antenna, MIMO ports placement.

I. INTRODUCTION

The rapid proliferation of wireless devices, insufficient bandwidth, and restricted channel capacity in the modern era have significantly boosted attempts to establish improved communication network standards. This has subsequently fostered the development of communication systems in next-generation (5G) at the mm-wave frequency, with significantly improved channel capacity and data rates [1], [2]. The next 5G technology offers not just a significant improvement to the safety and reliability of the connected devices, high data rates and low power consumption, But additionally, it offers new potential for emerging technologies, such as virtual realities and intelligent cities [3]–[5]. Aspects of the mm-wave spectrum that are critical to consider include signal fading, atmospheric absorption, and path loss attenuations, which become more important when using a single antenna [6], [7], that must nonetheless be addressed.

The associate editor coordinating the review of this manuscript and approving it for publication was Pavlos I. Lazaridis.

Multiple-input multiple-output (MIMO) antenna has been identified as a key technology for existing and future wireless systems that demonstrates the simultaneous operations of multi-antennas and increases channel capacity with high data rates and Gigabits/sec throughput [8]–[12]. The MIMO antenna of the 5th generation demands a wide bandwidth to operate concurrently, whereas the high gain is needed in order to decrease air losses, absorptions, and compactness of structure for assimilation in MIMO systems is needed. In addition, there are challenges with the MIMO antenna design, including the design of antenna elements placed close together and with low mutual coupling and strong isolation, which improves the antenna efficiency.

Patch antennas have garnered considerable interest due to their planar, compact, and resilient shapes in wireless systems and integrated circuits. The primary restrictions are lower gain and bandwidth that are greatly enhanced using various ways [13]–[15]. In contrast to the traditional methods mentioned previously for improving the defects of the patch antenna, we will use in this article a non-traditional form of the patch with high performance, which is the planar Spiral antenna.

A spiral antenna was first applied in the 1950s to obtain a frequency-independent antenna; it was defined in this context as an antenna that has an input impedance and gain that remain relatively constant throughout the bandwidth [16], [17]. This antenna has now become widely used in such sectors as military, satellite, telemetry, GPS, medical devices, wearable wireless communication and other wireless communication. A spiral antenna is noted for being adaptable in numerous applications, such as 5G wireless communications, which require large bandwidth, high gain and circular polarization. The Archimedean spiral, logarithmic spiral, square spiral, and star spiral are the numerous varieties of spiral antenna design. The most prevalent configurations are logarithmic spiral and Archimedean spiral.

There have lately been reports in literature on a variety of designs of MIMO antennas for 5G mm wave applications [18]–[24]. A circular polarized MIMO antenna with four ports was reported in references [18]. The antenna elements surround the metamaterial surface in order to obtain better radiation properties; nonetheless, the usage of the parasite parasitic elements the design of the MIMO difficult. A 5G MIMO antenna with a wide frequency range from 23 to 40 GHz with an overall dimension of $81 \times 80\ mm^2$ has also been described [19]. Although the antenna has high bandwidth and MIMO capabilities, they are expensive. The aforementioned [20] article offered an 8×8 MIMO antenna that measured $31.2 \times 31.2 \times 1.57\ mm^3$ in volume, and had a total gain of 8.732 dB with a center frequency of 25.2 GHz. This proposed antenna had an awful number of side and back lobes, which decreased its performance. In [21], an EBG-based MIMO antenna with a bandwidth of 0.8 GHz is reported. Reference [22] has a multi-element antenna design that directs the radiation in a direction that is suited for 5G communications. There is a 1.5 GHz bandwidth ranging from 27.2 GHz to 28.7 GHz, while the greatest gain achieved is 7.41 dB at 28 GHz. Another useful MIMO antenna option, designed for 5G, is a 4-element T-shaped antenna with total dimensions of $12 \times 50.8 \times 0.8\ mm^3$ [23]. The bottom layer partial ground is made up of iteratively inserted symmetrical split-ring slots. The proposed antenna design operates between 25.1 and 37.5 GHz and has a peak gain of 10.6 dBi. However, this study examines solely ECC as a MIMO performance measure. The work in point [24] also offers a high-gain fabry-perot antenna for 5G MIMO applications, which includes a superstrate. The structure suggested spans the spectrum of mm-waves from 26–29.5 GHz and the highest gain value is 14.1 dBi. Additionally, ECC is studied to determine the MIMO performance of the antenna design.

Although the literature proposes numerous MIMO antenna designs, a lack of systematic design approach and a lack of understanding about performance constraints are still present. In this work, we have utilized the theory of characteristic mode (TCM) as a very effective analytical and systematic technique in the MIMO antenna design. The feature of a major contribution is that it may provide us access to the many characteristics that characterize the antenna without having to excite the antenna.

The theory of characteristic modes is a modal analysis approach for antennas of any shape that was first established by Garbacz in 1968 [25] and then revised by Harrington in 1971 [26], [27]. Antenna designers may now extract the Eigen responses of an antenna using characteristic mode analysis (CMA), a rich set of information that was previously only available for closed waveguides and resonant cavities. The availability of these Eigen responses might potentially provide fresh physical insights into antenna construction and analysis. The characteristic modes or characteristic currents can be derived by the eigenfunctions of the following particular eigenvalue equation:

$$X\left(\mathrm{J_n}\right) = \lambda_n R\left(\mathrm{J_n}\right) \tag{1}$$

where λ_n are the eigenvalues, J_n are the eigenfuncions or eigen currents, and R and X are the real and imaginary parts of the impedance parameter Z.

Another significant metric derived from eigenvalues is modal significance ($\mathrm{MS_n}$), which is defined as

$$\mathrm{MS_n} = |1/(1 + j\lambda_n)| \tag{2}$$

Modal significance vividly demonstrates how each mode is near to resonance at each frequency. It reaches a maximum value of 1 at its resonant frequency (when $\lambda_n = 0$) and then drops off as eigenvalues increase.

One alternative to specifying the eigenvalues is to express them in terms of characteristic angle β_n. Characteristic angle can be delineated according to the following equation [28]:

$$\beta_n = 180^\circ - tan^{-1}\left(\lambda_n\right) \tag{3}$$

Characteristic angle has the advantage that their value change more quickly, making them ideal for analysis.

TABLE 1. Summary of three coefficients of characteristic modes.

Eigenvalue (λ_n)	Modal significance (MS_n)	Characteristic angle (β_n)	Mode Status
$\lambda_n > 0$	$0 < MS_n < 1$	$90^\circ < \beta_n < 180^\circ$	Inductive
0	1	180°	Resonant
$\lambda_n < 0$	$0 < MS_n < 1$	$180^\circ < \beta_n < 270^\circ$	Capacitive

Physically, the characteristic angle is a representation of the phase difference between the characteristic current J_n, and the corresponding characteristic field E_n. When $\lambda_n = 0$ which is refer to the characteristic angle $\beta_n = 180^\circ$, a specific mode resonates. It is important to note that if the characteristic angle is equal to 180°, the excited mode radiates effectively. In cases when β_n is close to 90° or 270°, the majority of energy is stored in the mode. Table. 1 summarize the scenario with eigenvalues λ_n, modal significance MS_n and characteristic angles β_n in the following manner:

The novelty/contribution of this work boils down to the following: Instead of the traditional shapes of the patch, such as the square, rectangular, triangle and circular shapes previously used in some designs, but in this manuscript, a novel logarithmic spiral patch has been used to obtain the circular polarization with acceptable performance more easily than the traditional shapes used before. In this manuscript, a systematic design of four configurations of a two-port novel logarithmic spiral MIMO array patch antenna was presented based on the theory of characteristic modes, which gives a physical insight into how the design is done and how to improve its performance. The novelty of this work is to abolish the idea of trials and error, which wastes a lot of time in the design process without understanding the mechanism of the work of the antenna, and thus improving it will be more difficult and take a lot of time. Therefore, this paper gives designers a vision of how to design the MIMO antenna in four different configurations and get the required results based on the required application in a faster time and with better performance than traditional methods. The design process begins with the support of characteristic mode analysis, starting with the design of a novel single element with one logarithmic spiral arm and then adding another arm to increase the bandwidth of the antenna, and then using the two-element array to increase the gain of the antenna, and ending with the design of four configurations of a two-port MIMO antenna, and the best performance out of those four., and all this will be presented in Section II. While in Section III the fabricated antennas will be presented and comparing this proposed antenna with state-of-the-art works. Lastly, Section IV provides the conclusion.

II. ANTENNA DESIGN PROCEDURE

A complete strong look at the design's growth based on the characteristic mode analysis, starting from a single element, passing through a two-element array antenna, and ending in a MIMO configuration is extensively detailed in the ensuing. Antenna modeling, analysis, and simulation are done in the CST microwave studio suite, which is a commercially accessible EM simulator.

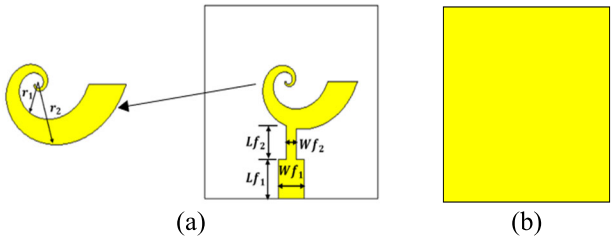

FIGURE 1. One arm logarithmic spiral patch antenna, (a) Top view, (b) Bottom view (full metallic ground plane).

A. SINGLE ELEMENT LOGARITHMIC SPIRAL PATCH ANTENNA

5G wireless communication requires high performance antennas with features such as high gain, large bandwidth, and circular polarization. Therefore, in this article, we have chosen the logarithmic spiral patch antenna as shown in Figure 1 because it gives the required specifications and performance for wireless 5G applications, as mentioned earlier in the introduction part. But at first, the characteristics of this logarithmic spiral patch must be studied using CMA to ensure its performance and identify the factors that must be improved in a systemic, easy, and time-saving manner.

The one arm logarithmic spiral antenna was designed using the equations $r_1 = r_o e^{a\theta}$ and $r_2 = r_o e^{a(\theta-\theta_o)}$, where r_1 and r_2 are inner radius and outer radius of the spiral respectively, while r_o is the initial radius, θ is the incremental angle, a is the progression factor, and θ_o is the phase shift of the spiral. A fast optimization of the logarithmic spiral antenna with initial radius $r_o = 0.15$ mm, incremental angle $\theta = 5°$, progression factor $a = 0.35$, and the phase shift $\theta_o = 90°$ is verified by modal significance (MS) and characteristic angle (CA) as indicated in Figure 2. The modal significance and characteristic angle are the two parameters that dictate the radiation performance of each mode, notably the circular polarization radiation generated by two modes. As a result, the specifications for these two modes are as follows: (a) the modal significances of the two orthogonal modes are identical (the two modes' normalized amplitudes are identical), and (b) the characteristic angles of these modes are $\beta_1 = 135°$ and $\beta_2 = 225°$, a difference of 45 ° from the operating angle mode of 180 °. Figure 2 presents the MS and CA of the first five modes. In all CMA results, J_1 to J_5 denote to the first CM to the five CM. As can be seen, the magnitudes of modes J_1 and J_2 are almost the same and they present a phase difference of 87.5° in the desired operating frequency 28 GHz. Thus, it is possible to get a CP antenna after the proper feeding.

The type of circular polarization, whether it is right- or left-handed, may be determined quite easily by characteristics mode analysis. It is the phase difference's sign that determines the rotation's handedness Left-handed polarization with a phase shift of +90° is achieved by rotating counterclockwise. Right-handed polarization is achieved by rotating clockwise with a -90° phase shift. As can be seen

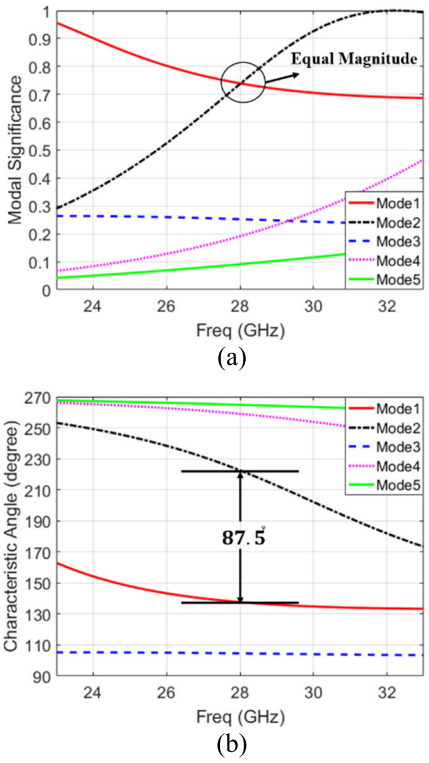

FIGURE 2. Modal significance and characteristic angle of the first five modes of one arm logarithmic spiral patch antenna.

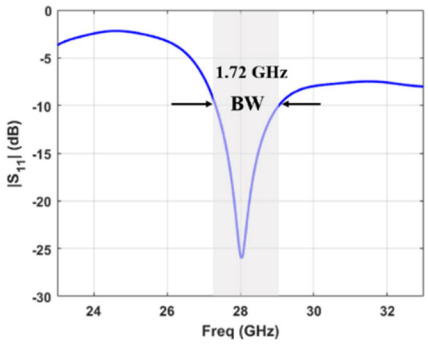

FIGURE 3. Simulated $|S_{11}|$ of one arm logarithmic spiral patch antenna.

in Figure 2b, the phase shift between modes 2and mode 1 is near to +90 degrees, and as a result, we can claim that this logarithmic spiral patch antenna has a left-hand circular polarization (LHCP). This was the motivation behind selecting a logarithmic spiral shape for the patch rather than the typical geometries described in the literature review, which made it easier to generate circular polarization.

After the proper quarter-wave impedance transformer feed as introduced in Figure 1a, the proposed one arm logarithmic spiral patch is excited to resonate at the resonating frequency of 28 GHz with a bandwidth of about 1.7 GHz as shown in Figure 3.

It is necessary to increase both the impedance and the axial ratio bandwidths of this antenna in a systematic way to meet the requirements of 5G wireless communication. Therefore, we will use an additional logarithmic spiral arm, as shown in Figure 4. Figure 4 depicts a spiral antenna with

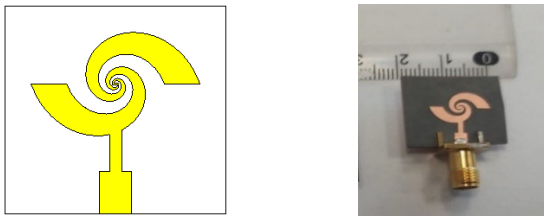

FIGURE 4. Two arm logarithmic spiral patch antenna.

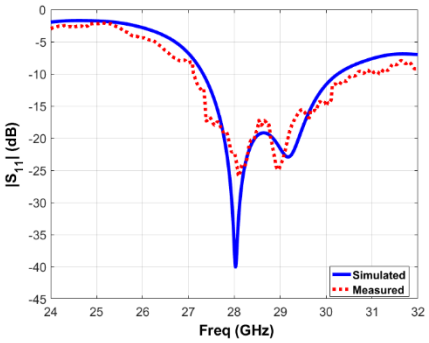

FIGURE 5. Simulated and measured $|S_{11}|$ of two arm logarithmic spiral patch antenna.

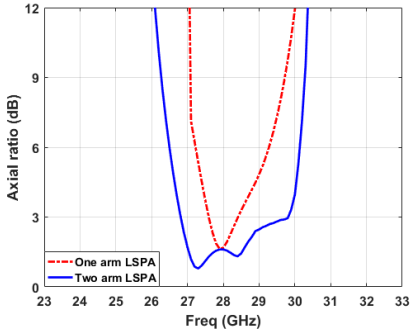

FIGURE 6. Simulated axial ratio (dB) of the one-arm and two-arm logarithmic spiral patch antennas.

two equal arms, each with a 1.5 turn. These two spiral arms are connected to each other by a rectangular strip that has a length of 0.48 mm and a width of 0.15 mm. The simulated and measured reflection coefficient curve of the two-arm logarithmic spiral patch antenna is shown in Figure 5. It is evident from Figure 5, the bandwidth has doubled to 3.07 GHz compared to the bandwidth of the one arm logarithmic spiral patch antenna.

Figure 6 shows a comparison of the simulated axial ratio between the one-arm and two-arm logarithmic spiral patch antennas. When comparing the two-arm logarithmic spiral patch antenna to the one-arm antenna, the gain in axial ratio bandwidth is up to 250 % more. The addition of a logarithmic spiral arm not only increased the bandwidth of the antenna, but it also increased its gain. When using only one arm, the gain of the logarithmic spiral patch antenna is reported to be 6.2 dB, which increases to 7 dB when using the patch antenna with two arms.

Figure 7 depicts the two-arm logarithmic spiral patch antenna's E- and H-plane radiation patterns at the operating frequency of 28 GHz. The right-hand CP (RHCP) is very

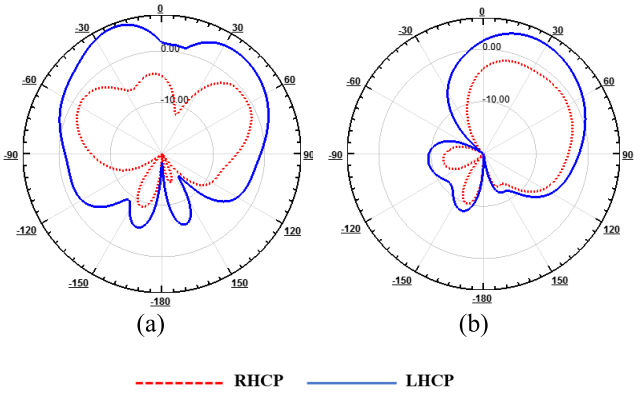

FIGURE 7. Simulated far-field radiation patterns of the two-arm logarithmic spiral patch antenna. (a) E-plane, (b) H-plane.

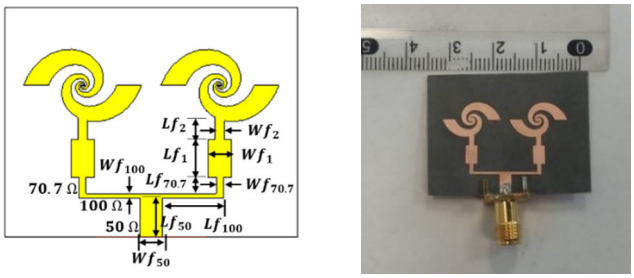

FIGURE 8. Two element array logarithmic spiral patch antenna.

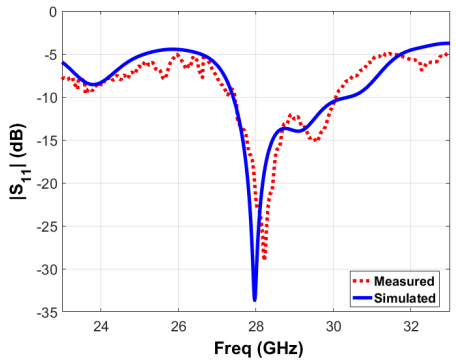

FIGURE 9. Simulated and measured $|S_{11}|$ of two element array spiral logarithmic spiral patch antenna.

small in comparison to the left-hand CP (LHCP). In the E and H planes, the RHCP level is around 12 dB lower than the LHCP level. In other words, the antenna exhibits LHCP in the main lobe direction.

B. TWO ELEMENT ARRAY LOGARITHMIC SPIRAL PATCH ANTENNA

At mm-wave frequencies, the gain of the antenna must be sufficient to compensate for the increased attenuation and absorption caused by the atmosphere. Nevertheless, the single-element antenna yielded in this study offers insufficient gain. Therefore, as shown in Figure 8, with the addition of a corporate feed network, the design has been developed into a two-element array. The array's elements are connected by a T-junction-power divider feed network, where the network's feed line widths are intended to match at 50 Ω with the main feed but 100 Ω with the branching network. The

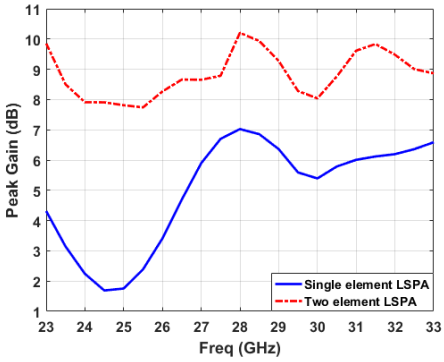

FIGURE 10. Gain vs. frequency of single-element and two-element array antennas.

TABLE 2. The proposed antenna's optimum values (in millimeter).

Par.	value	Par.	value	Par.	value
Single-element logarithmic spiral patch antenna					
Wf_1	2.47	Wf_2	1	Lf_1	3.264
Lf_2	3.2	θ	5	θ_o	90
r_o	0.15	a	0.35		
Two-element array logarithmic spiral patch antenna					
Wf_{50}	2.47	Wf_{100}	0.5	$Wf_{70.7}$	0.8
Lf_{50}	4.2	Lf_{100}	6.6	$Lf_{70.7}$	1.8
S	18				

array's two elements are spaced by a distance of 2 mm. which is approximately equal to 0.2λ at 28 GHz. The parameters for the optimal performance of the proposed antenna are obtainable in Table. 2. The simulated and measured reflection coefficient curve of the two-element array logarithmic spiral patch antenna is shown in Figure 9. It is apparent that the two-element array antenna operates in the 27.4-30.47 GHz mm-wave frequency range, with a bandwidth of 3.07 GHz. When a two-element array antenna is produced from a single-element antenna, the appearance of bandwidth gain is evident.

A comparison of the broadband gain between single element and two-element array logarithmic spiral patch antennas is shown in Figure 10. The simulated broadband gain increases from 7 dB to 10.2 dB when the single element antenna is turned into a two-element array antenna, as shown in Figure 10.

Figure 11 presents the radiation patterns of the two-element array logarithmic spiral patch antennas at 28 GHz for both the E- and H-planes. It could be observed that the two-element array antenna exhibits radiation patterns with left-hand CP (LHCP) radiation for both the E-and H-planes. The comparison of the simulated axial ratio for the single-element and two-element array antennas are shown in Figure 12. It was observed that there was a modest increase in the axial ratio bandwidth when the single-element antenna was modified to become a two-element array antenna.

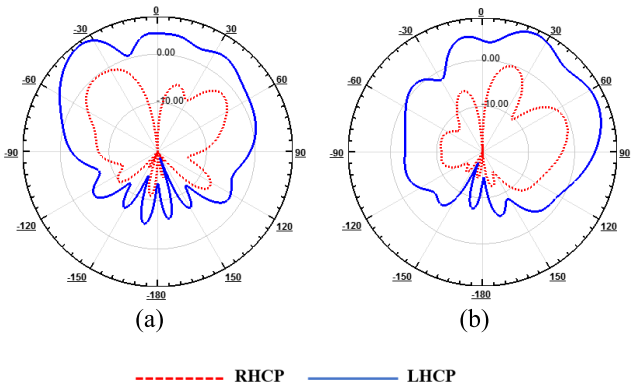

FIGURE 11. Simulated far-field radiation patterns of the two-element array logarithmic spiral patch antenna (a) E-plane, (b) H-plane.

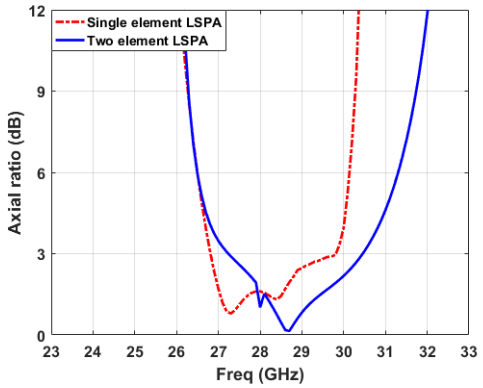

FIGURE 12. Simulated axial ratio (dB) of the single-element and two-element array antennas.

III. MIMO ANTENNA CONFIGURATIONS

After acquiring a two-element array, the design will be further developed, culminating in the creation of the four different configurations of the 2-port MIMO antenna system as indicated in Figure 13. Therefore, in this study, with the help of the characteristic mode analysis, we will make a comparison between these different configuration systems to select the best one in performance.

A. SYSTEM-1: FACE-TO-FACE MIMO LOGARITHMIC SPIRAL PATCH ANTENNA

Figure 13 (a) depicts the geometry of the face-to-face 2-port MIMO logarithmic spiral patch antenna, which is also referred to as a system-1 antenna. The designed antenna's substrate is a Rogers RT5880 with a relative permittivity (ε_r) of 2.2, a loss tangent of 0.0009, and a thickness of 0.787 mm. The whole area of design was 32 $\times$ 43 mm^2. The CMA approach has been applied to MIMO System-1, with its substrate included, as shown in Figure 13. In Figures 14 and 15, the modal significance MS and the modal current distribution curves at 28 GHz are depicted. As we can see in Figure 10, modes 1, 2, 3, 4, and 5 contribute to the radiating BW in the desired impedance BW of interest (MS $\geq$ 0.707), whereas mode 6 has no effect whatsoever. According to the current directions, we may note from Figure 11 that modes 1 and 2 do not contribute to the coupling between the two antennas,

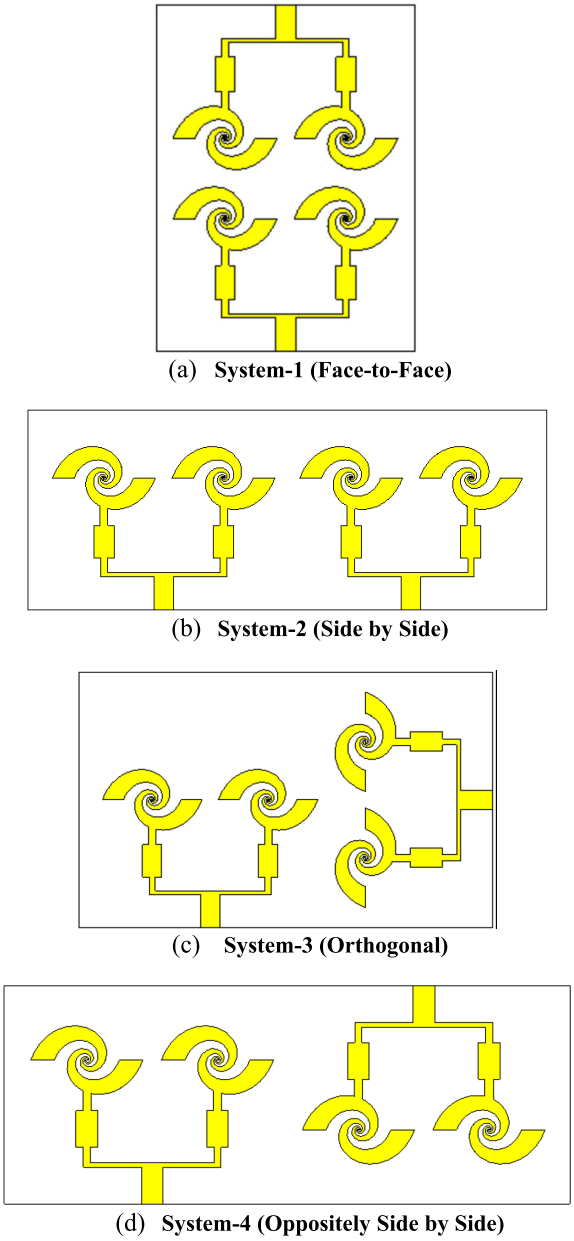

FIGURE 13. MIMO antenna configurations.

while modes 3, 4, and 5 cause the coupling between the two antennas, which in turn negatively affects the performance of this MIMO antenna system. According to our study, we are able to draw the conclusion that radiation is caused by either Mode 1 or Mode 2, or a combination of both.

The simulated s-parameters, including the S_{11} and S_{21} curves of the face-to-face 2-port MIMO antennas, are presented in Figure 16. The simulated impedance BW (VSWR $<$ 2, -10 dB) of this system was 3.0341 GHz, ranging from 27.467 to 30.501 GHz, while a simulated isolation of -21.1 dB was accomplished between the System-1 antennas. This poor isolation was expected by the modal significance curve (Figure 14), and this was confirmed by the S-Parameters curve (Figure 16), which negatively affects the performance of this system.

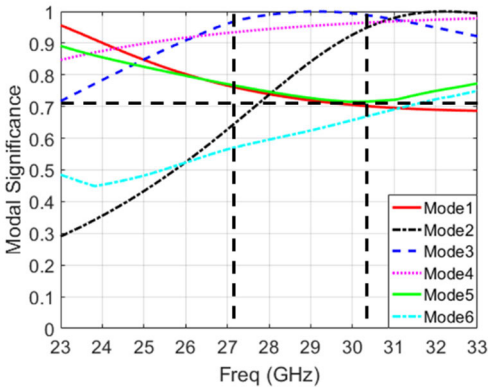

FIGURE 14. Modal significance curves of the face-to-face 2-port MIMO antenna.

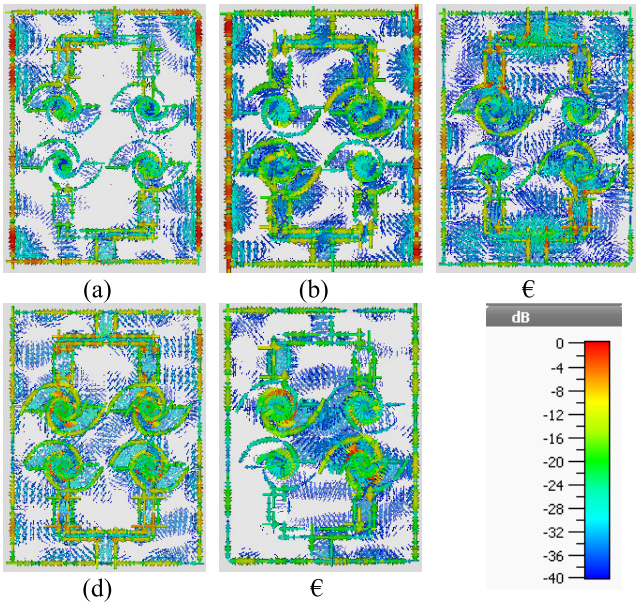

FIGURE 15. The first five modes' current distribution of the face-to-face 2-port MIMO antenna system, where (a) mode 1 (b) mode 2 (c) mode 3 (d) mode 4 (e) mode 5.

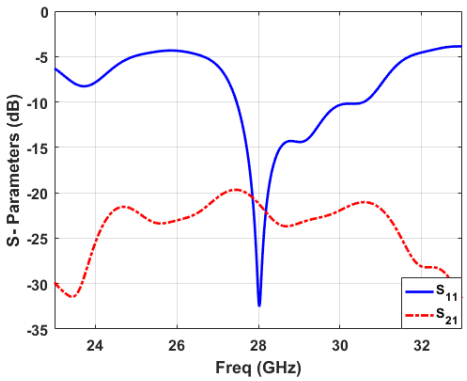

FIGURE 16. S-Parameters of the face-to-face 2-port MIMO antenna (System-1).

B. SYSTEM-2: SIDE BY SIDE MIMO LOGARITHMIC SPIRAL PATCH ANTENNA

Figure 13 (b) depicts the geometry of the Side by Side 2-port MIMO logarithmic spiral patch antenna, which is also referred to as the System-2 antenna. As with the System-1 antenna, the System-2 antenna was designed using the same substrate properties. The total designed area was 65×25 mm^2. Like the System-1 2-port MIMO antenna design, CMA was also applied to the Side by Side 2-port MIMO antenna, including the substrate. Figs. 17 and 18 present the 28 GHz modal significance and the modal current distribution curves. From Figure 17, it is interesting to note that modes 1, 2, 3, and 4 contribute to the radiating BW of interest (MS $\geq$ 0.707), while modes 5 and 6 have no effect on the required impedance BW. Figure 18 shows that modes 1 and 2 have a current null between the two antennas, but modes 3 and 4 have a current coupling between the antennas. There are two non-coupling modes, mode 1 and mode 2, as well as coupling modes 3 and 4. It is also clear from Figure 18 that this coupling is a horizontal coupling, which has less impact on the antenna performance than the vertical coupling occurring in the face-to-face 2-port MIMO antenna system.

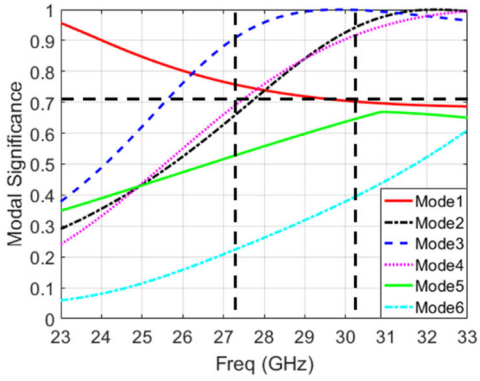

FIGURE 17. Modal significance curves of the side by side 2-port MIMO antenna system.

From the S-parameters plotted in Figure 19, the isolation is better between the side by side 2-port MIMO antenna system than between the face-to-face 2-port MIMO antennas. Therefore, it is expected that this system will give better and higher performance than System-1 antenna.

C. SYSTEM-3 (ORTHOGONAL) MIMO LOGARITHMIC SPIRAL PATCH ANTENNA

As shown in Figure 13 (c), the System-3 antenna is an orthogonal 2-port MIMO logarithmic spiral patch antenna. As with System-1 and System-2, the System-3 antenna was designed with the identical specifications of the substrate. The total design area was 53.5×33 mm^2. CMA was also used on the orthogonal 2-port MIMO antenna, including the substrate, as it was on the face-to-face and side by side 2-port MIMO systems. It is noteworthy to notice that modes 1, 2, 3, and 4 all contribute to the radiating BW of interest (MS $\geq$ 0.707), whereas modes 5 and 6 have no effect on the needed impedance BW, as shown in Figure 20. From Figure 21, we may conclude that modes 1 and 2 have no impact on the coupling between the two antennas, but modes 3, and 4 are responsible for the coupling between the two antennas, and the poor performance of this MIMO antenna system.

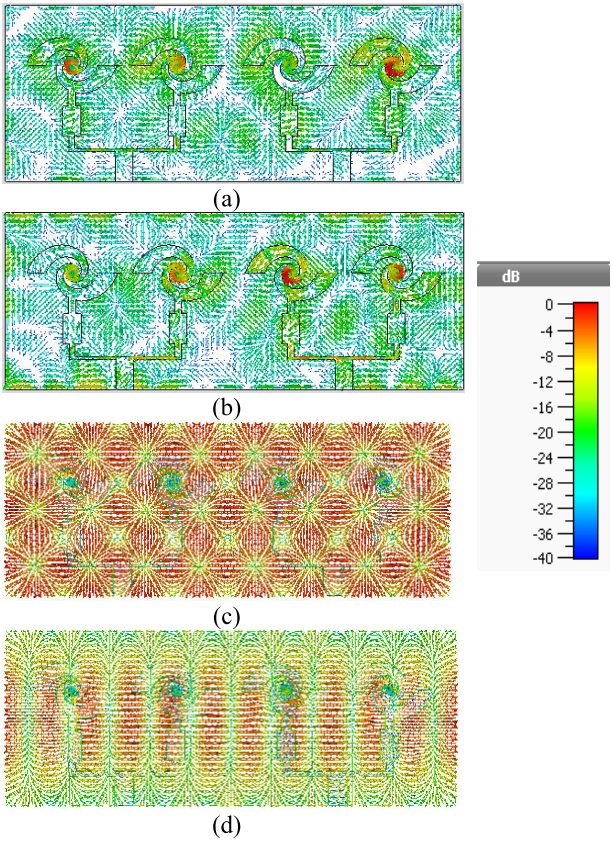

FIGURE 18. The first four modes' current distribution of the side by side 2-port MIMO antenna system, where (a) mode 1 (b) mode 2 (c) mode 3 (d) mode 4.

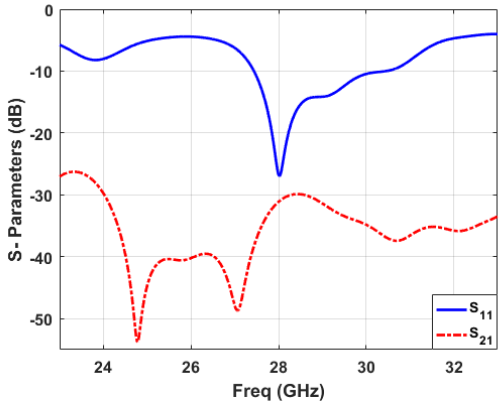

FIGURE 19. S-Parameters of the Side by Side 2-port MIMO antenna (System-2).

According to the S-parameters plotted in Figure 22, the isolation between the orthogonal 2-port MIMO antenna system is better than the isolation between the antennas of System-1, but it has lower isolation than the antennas of System-2. As a result, it is anticipated that this system will provide better and greater performance than the competing System-1 antenna.

D. SYSTEM-4 (OPPOSITELY SIDE BY SIDE) MIMO LOGARITHMIC SPIRAL PATCH ANTENNA

The geometry of the oppositely side by side 2-port MIMO logarithmic spiral patch antenna, also known as the System-4 antenna, is shown in Figure 13(d). As with the prior systems, the antenna was developed to the same specifications as the substrate, with a total design area of 65 × 25 mm^2. CMA was also applied to the System-4 antenna, including the substrate, as was the case with earlier systems. Figure 23 shows that only modes 1, 2, and 3 contribute to the target impedance BW (MS ≥ 0.707), but modes 4, 5, and 6 are entirely unnecessary. We can see from Figure 24 that modes 1 and 2 do not contribute to the coupling between the oppositely side by side MIMO antennas (As a result of the existence of current nulls). However, mode 3 is producing poor coupling between the oppositely side by side MIMO antennas. As it is clear from the CMA, only one mode (mode 3) causes a poor coupling between the antennas, and this system is expected to be the best in performance, and this is what was shown by the S-parameters curve in Figure 25.

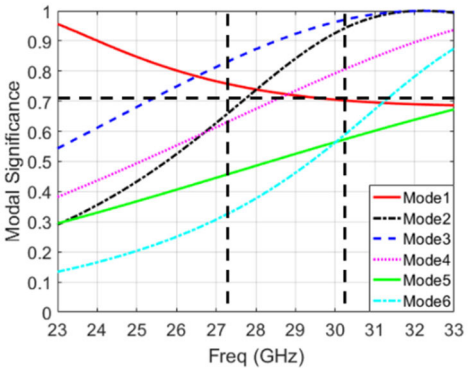

FIGURE 20. Modal significance curves of the orthogonal 2-port MIMO antenna system.

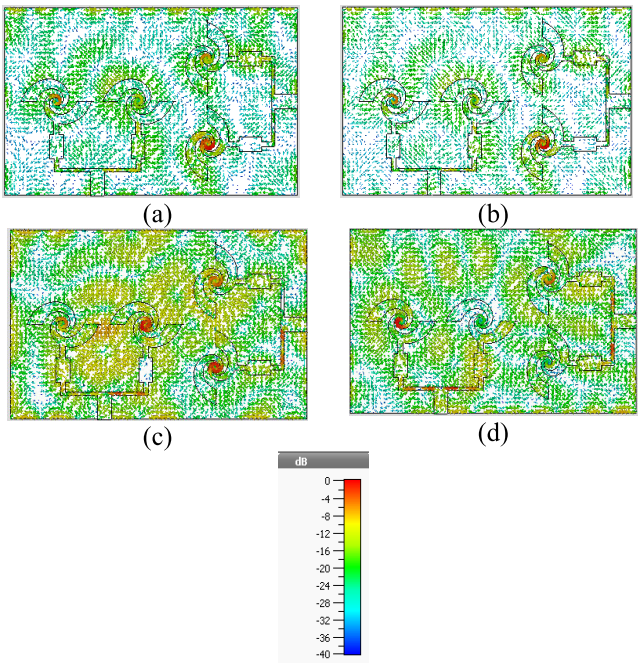

FIGURE 21. The first four modes' current distribution of the orthogonal 2-port MIMO antenna system, where (a) mode 1 (b) mode 2 (c) mode 3 (d) mode 4.

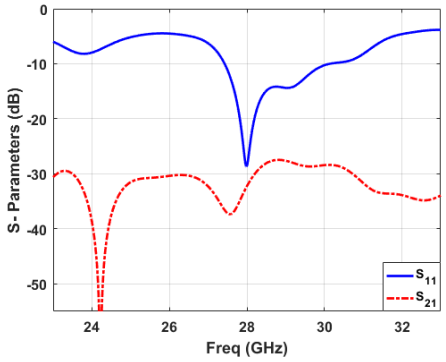

FIGURE 22. S-Parameters of the orthogonal 2-port MIMO antenna (System-3).

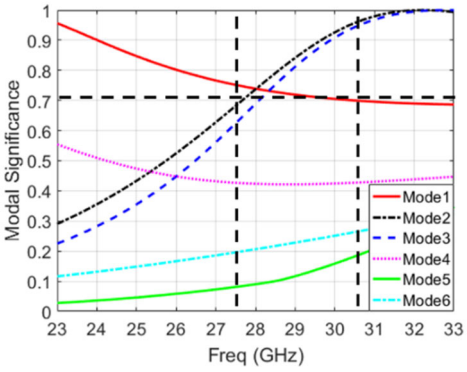

FIGURE 23. Modal significance curves of the oppositely side by side 2-port MIMO antenna system.

E. COMPARISON BETWEEN THE DIFFERENT SYSTEMS OF ANTENNA

This section deals with a brief comparison between the previous four different systems to determine the best performing system. This comparison is summarized in Table 3, in terms of the number of modes that cause coupling between the MIMO ports, impedance BW, gain, envelope correlation coefficient (ECC), channel capacity loss (CCL), and axial ratio bandwidth. As it is evident from Table 3, the MIMO antenna system that has the least mutual coupling has the best performance, and this is represented by the lowest ECC, the lowest channel capacity loss (CCL), and the highest gain. Therefore, system 4, which is namely the Oppositely side by side 2-port MIMO antenna, has only one mode that causes the lowest coupling between MIMO ports, unlike other systems that have more than two modes, which cause high coupling between MIMO ports, and this negatively affects the performance of these systems. System 4 exhibits the highest value of S_{21}, indicating its high isolation, wider BW, and highest system gain. Therefore, based on this study, which is completely based on characteristic mode analysis, system 4 is the best in performance.

F. THE PROPOSED 2-PORT MIMO ANTENNA SYSTEM

As it is clear from Figure 24, there is only one mode (mode 3) that causes coupling between the MIMO antenna ports, so we must block this mode without affecting the non-coupling modes (mode1 and mode 2), so we will use the connected five circular Ring Defected Ground structure

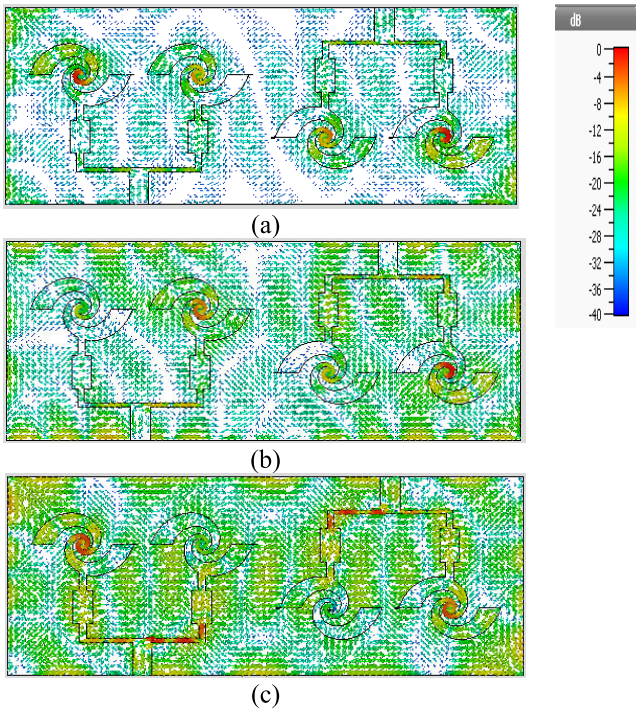

FIGURE 24. The first three modes' current distribution of the oppositely side by side MIMO antenna system, where (a) mode 1 (b) mode 2 (c) mode 3.

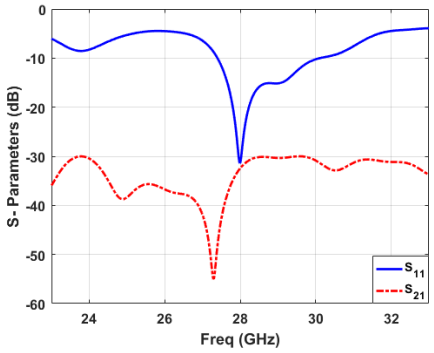

FIGURE 25. S-Parameters of the Oppositely side by side 2-port MIMO antenna (System-4).

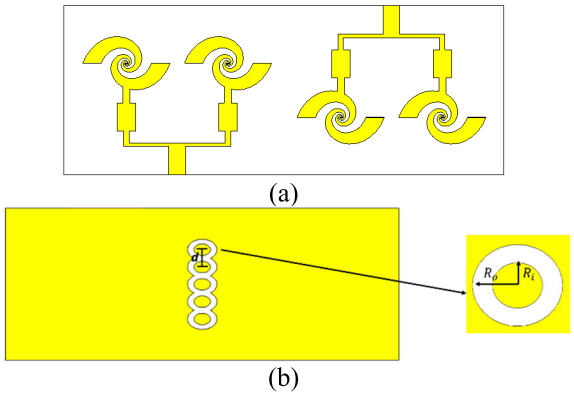

FIGURE 26. Proposed MIMO antenna configuration. (a) Top view, (b) Bottom view.

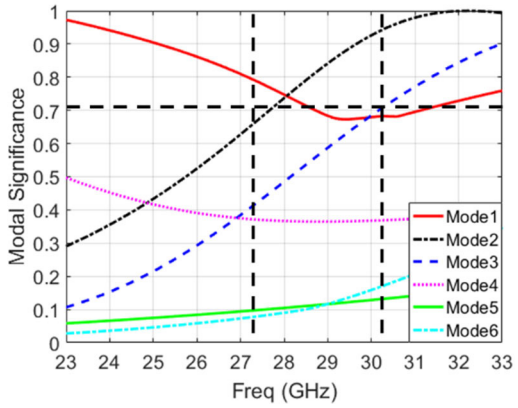

FIGURE 27. Modal significance curves of the proposed oppositely side by side 2-port MIMO antenna system with DGS.

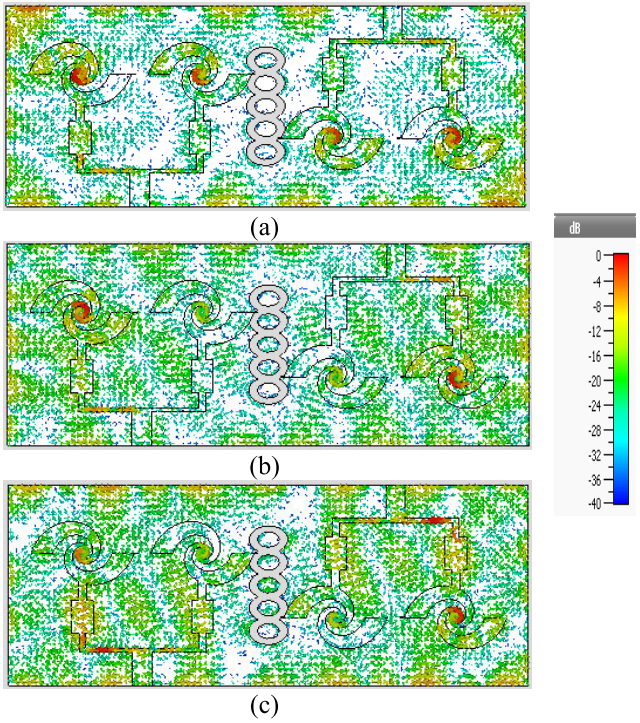

FIGURE 28. The first three modes' current distribution of the proposed oppositely side by side 2-port MIMO antenna system with DGS, where (a) mode 1 (b) mode 2 (c) mode 3.

to perform this task. The concept is easy to understand if we consider the desired bandwidth to have two modes, one that is coupling and one that is non-coupling, which can be completely blocked without causing the other to be hindered. When it comes to extra modes, though, it becomes much more difficult. For the concept to be proven and adapted to any design, a single ring DGS structure was not suitable. So instead, a DGS structure comprised of connected five rings with center-to-center distance $d = 2.85$ mm as shown in Figure 26 would be the best way to show the principle and generalize it to any design, regardless of antenna type. On the whole, DGS's inner and outer radiuses have been designed to optimize for the proposed operating frequency band. It will also save the designer time on optimization. As a result,

TABLE 3. Comparison between the different MIMO antenna systems.

	# of coupling modes	Isolation (dB)	BW (%)	Gain (dB)	ECC	CCL (bit/s /Hz)	Axial ratio BW (%)
Sys.1	3	19	10.8	8.5	0.15	0.4	9.3
Sys.2	2	29.5	11.4	9.5	0.02	0.19	10.1
Sys.3	2	28	11.6	8.8	0.05	0.25	10.4
Sys.4	1	30.5	11.9	10.1	0.01	0.11	11

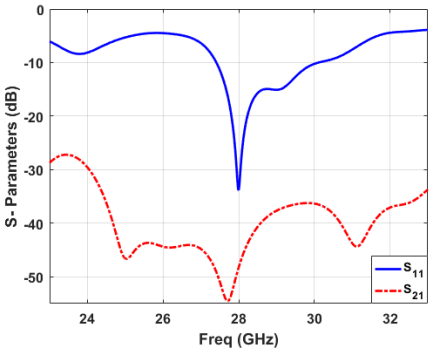

FIGURE 29. S-Parameters of the proposed oppositely side by side 2-port MIMO antenna with DGS.

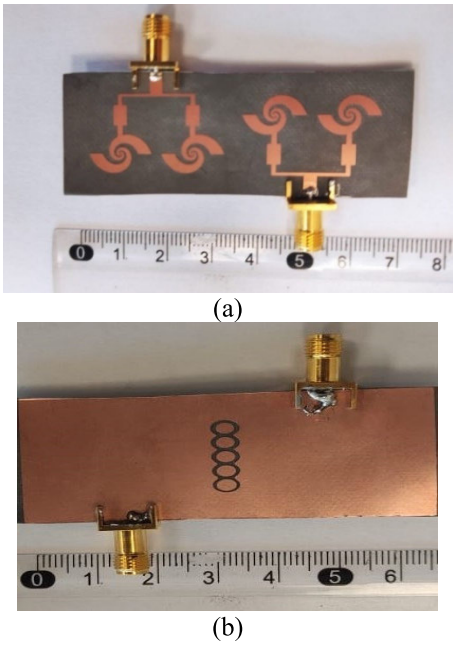

FIGURE 30. Fabricated prototype of the proposed MIMO antenna system (a) Top view (b) Bottom view.

the DGS was positioned in a central position on the ground plane between the two ports. The inner and outer radii are $R_i = 2.3mm$ and $R_o = 2.5mm$, respectively.

Discussing how the DGS influences the CM is essential before demonstrating the improvement in S-parameters. In Figures 27 and 28, the modal significance and current distribution plots at 28 GHz are displayed. Due to the fact that the DGS has been designed to be parallel to the current flow of the non-coupling modes, the modes 1 and 2 current distributions are not totally impacted, whereas the mode 3 current distribution is impacted and tuned out of the BW of interest (MS $\geq$ 0.707) because the DGS produces a current

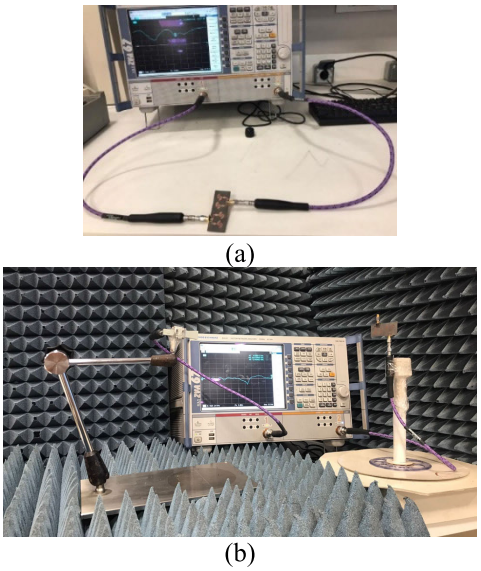

FIGURE 31. (a) S-parameters measurement setup. (b) Far-field measurement setup.

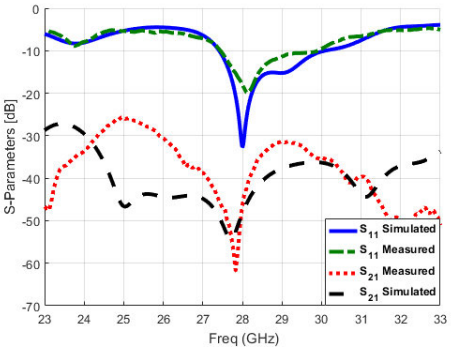

FIGURE 32. Measured and simulated S-Parameters of the proposed antenna.

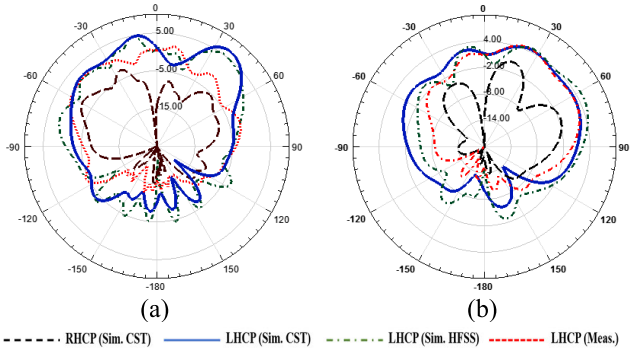

FIGURE 33. Simulated and measured far-field radiation patterns of the proposed antenna. (a) E-plane, (b) H-plane.

that flows in the opposite direction to the coupling mode's initial current flow.

The S-parameters curve of the proposed oppositely side by side 2-port MIMO antenna with DGS is illustrated in Figure 29. We can see that a simulated isolation of −55 dB is obtained between the 2-port MIMO antenna. According to our estimates, the frequency BW has been reduced by 200 MHz, with the primary reason appearing to be the blocking of mode 3.

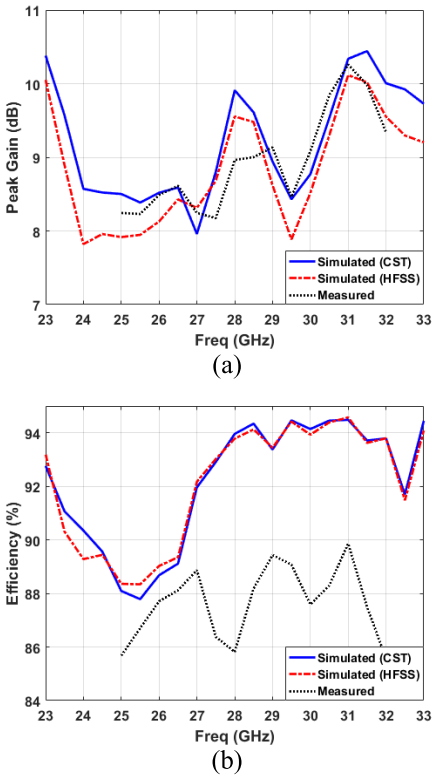

FIGURE 34. (a) Simulated and measured gain of the proposed MIMO antenna. (b) Simulated and measured efficiency of the proposed MIMO antenna.

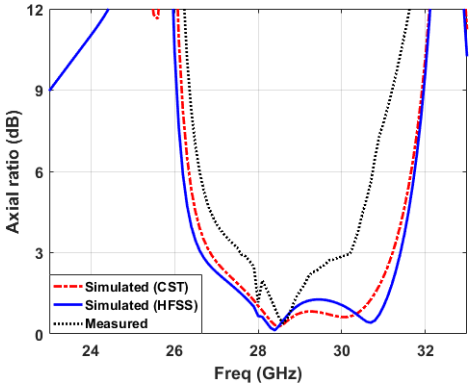

FIGURE 35. Simulated axial ratio (dB) of the proposed oppositely side by side 2-port MIMO CP antenna.

IV. EXPERIMENTAL RESULTS

The proposed system prototype of the oppositely side by side 2-port MIMO logarithmic spiral patch antenna was fabricated using the photo-lithographic method, and measured using a vector network analyzer (VNA), R&S ZVA 67, in order to verify the simulation results. The far-field measurement was performed using the VNA in two-port measurement mode by measuring the transmission coefficient $|S_{21}|$ between the antenna under test and the reference-standard gain horn antenna (LB-018400). Figures 30 and 31 depict the fabricated prototype of system as well as the measurement setup for the proposed antenna system. The following sections give a full description and comparative analysis of the measured results.

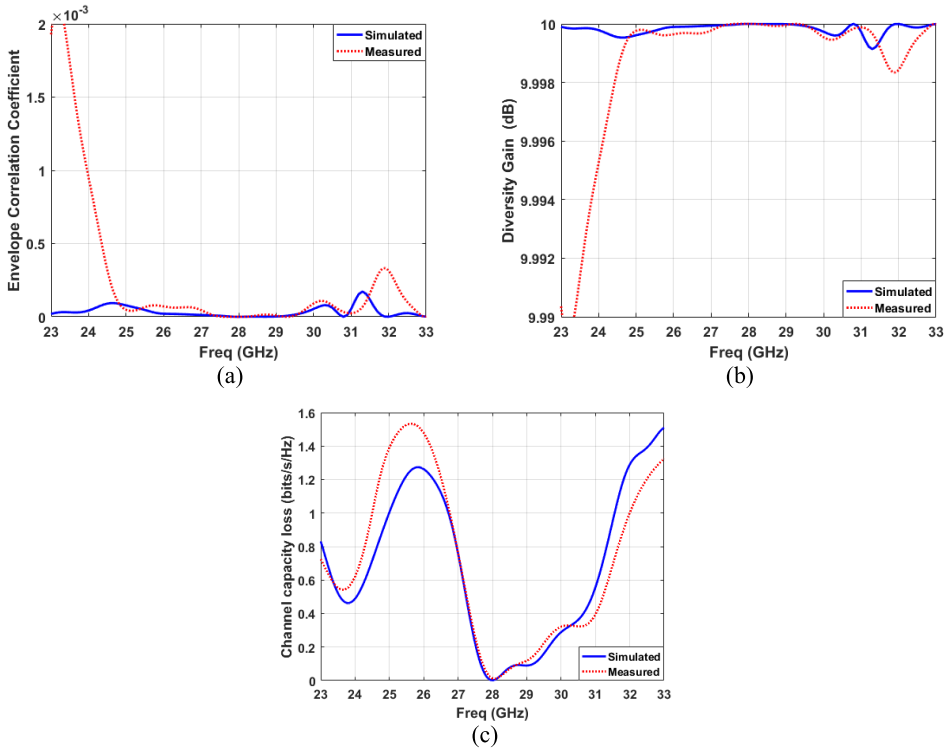

FIGURE 36. The proposed MIMO antenna performance parameters. (a) ECC (b) DG (c) CCL.

A. SCATTERING PARAMETERS

Figure 32 compares reflection S_{11} and transmission S_{21} coefficients based on simulated and measured values. It was found that the measured bandwidth was approximately 2.95 GHz (27.35-30.3 GHz), which is in excellent accordance with the simulated result. It has been noted that the antenna has good isolation characteristics, with values ranging from −54.5 to −36 dB. It finds a minor disparity between the simulated and measured outcomes. This discrepancy is primarily the result of fabrication and measurement setup flaws.

B. RADIATION PATTERNS

Figure 33 depicts the proposed oppositely side by side 2-port MIMO antenna system radiation patterns, which were simulated in both CST and HFSS software and measured at the resonating frequency of 28 GHz, in both principal planes of Phi = 0 and Phi = 90. Because of their oppositely side by side placement, the radiating elements of the proposed MIMO antenna exhibit pattern diversity, which is beneficial in reducing the multipath effect in communication systems. The directional radiation patterns of the MIMO antenna system are visible. The simulated and measured radiation patterns match up quite well with the antenna's suggested design. Figure 34 shows the simulated and measured gain and radiation efficiency of the proposed oppositely side by side 2-port MIMO antenna design. In the band of interest (27.3–30.3 GHz), the simulated gain fluctuates between 8.5 and 9.9 dBi, while the measured gain fluctuates between 8.2 and 9.5 dBi. The simulated radiation efficiency varies between 92 and 94 percent, while the measured radiation efficiency varies between 86 and 89 percent. As a result, the loss tangent of the Rogers dielectric material is 0.0009, which yields these high-efficiency results.

The proposed oppositely side by side 2-port MIMO CP antenna's simulated and measured axial ratios are shown in Figure 35. Figure 35 shows that the simulated (both with CST and HFSS) and measured axial ratio are roughly 0.66 dB at 28 GHz, suggesting that the resulting circular polarization is fairly satisfactory, while the ideal circular polarization has an axial ratio of 1 or 0 dB and is acceptable up to 3 dB [29].

C. MIMO PERFORMANCE PARAMETERS

In this part, we will discuss the essential performance parameters of a MIMO system. These characteristics are crucial to a MIMO system: the Envelope Correlation Coefficient (ECC), Diversity Gain (DG), and Channel Capacity Loss (CCL). The envelope correlation coefficient (ECC) describes the degree to which one antenna's performance is independent of the performance of another antenna. In ideal conditions, the value of ECC should be 0. Nonetheless, it is acceptable to have an ECC < 0.5 for practical purposes. The proposed oppositely side by side 2-port MIMO antenna's ECC can be computed using following expression [30]:

$$\mathrm{ECC} = \frac{\left|\iint_{4\pi} \left[\mathrm{A}_1(\theta,\varphi) * \mathrm{A}_2(\theta,\varphi)\right] \mathrm{d}\Omega\right|^2}{\iint_{4\pi} \left|\mathrm{A}_1(\theta,\varphi)\right|^2 \mathrm{d}\Omega \iint_{4\pi} \left|\mathrm{A}_2(\theta,\varphi)\right|^2 \mathrm{d}\Omega} \tag{4}$$

As shown in Figure 36.a, the ECC values for the proposed work were calculated using simulation and measurement data. As can be seen, the measured ECC is substantially

TABLE 4. Comparison of the performance of the proposed antenna to that of state-of-the-art works.

Refs	f_r (GHz)	Antenna Size	Separation Distance	Isolation Criteria	Isolation (dB)	Polarization Type	3dB Axial ratio Bandwidth (%)	Impedance Bandwidth (%)	Gain (dB)	ECC/DG (dB)	CCL (bit/s/Hz)
[10]	28	1.86 λ × 1.68 λ × 0.023 λ	0.12 λ	Metal strips	24	LP	—	3.03	8	0.013/9.9	N/A
[11]	28	2.8 λ × 3.26 λ × 0.07 λ	1.02 λ	DGS	17	LP	—	14.6	8.3	0.01/9.96	0.4
[18]	27.5	1.1 λ × 1.1 λ × 0.046 λ	0.36 λ	Meta-surface	30	CP	16.8	23.6	11	0.015/9.91	0.19
[21]	24	1.52 λ × 1.21 λ × 0.02 λ	0.41 λ	EBG	37	LP	—	3.3	6	0.24/9.7	N/A
[23]	28	4.66 λ × 1.12 λ × 0.075 λ	1.18 λ	DGS	22	LP	—	44.28	10.6	0.01/ N/A	N/A
[31]	30	2 λ × 2 λ × 0.025 λ	0.5 λ	FSS	20	CP	16.4	19.3	8	N/A	N/A
[32]	28	1.71 λ × 1.11 λ × 0.09 λ	0.068 λ	MTM	21	LP	—	17.8	10	0.015/ N/A	N/A
[33]	28/38	2.34 λ × 0.99 λ × 0.073 λ	0.54 λ	Increase the spacing between the elements	30/25	LP	—	12.8/14.8	5/5.7	0.01/9.9	N/A
[34]	28/38	1.86 λ × 2.24 λ × 0.047 λ	N/A	Arrangement of the antenna elements	28/28	LP	—	3.57/3.15	7.1/7.9	0.001/ N/A	N/A
[35]	28	2.8 λ × 2.8 λ × 0.073 λ	N/A	Arrangement of the antenna elements	29	CP	4.9	7.14	6.1	0.16/ N/A	N/A
[36]	28	5.9 λ × 6.5 λ × 0.047 λ	0.75 λ	Arrangement of the antenna elements	20	LP	—	8.2	13.5	N/A	N/A
Proposed antenna	28	6 λ × 2.3 λ × 0.073 λ	0.3 λ	Arrangement of the antenna elements + DGS + CMA	36	CP	10.2	10.71	9.9	0.0002/9.99	0.1

smaller than 0.002, which is owing to the high degree of isolation between the MIMO radiating elements.

Diversity Gain (DG) is the loss in transmission power that happens when diversity methods are implemented in a MIMO antenna system. DG is also considered to be an essential characteristic for evaluating the performance of MIMO antenna systems. The formula in [30] can be used to calculate the DG value:

$$DG = 10\sqrt{1 - (ECC)^2} \tag{5}$$

As shown in Figure 36.b, all of the antenna ports have a diversity gain more than 9.995 dB, which is extremely close to the ideal value of 10 dB.

Channel Capacity Loss (CCL) is one of the most significant MIMO system metrics. CCL describes a potential loss of channel capacity due to correlation between the MIMO links. One method of calculating the CCL is provided in equation (6) as reported in [30].

$$CCL = -\log_2[\det(a)] \tag{6}$$

where $a = \begin{bmatrix} \sigma_{11} & \sigma_{12} \\ \sigma_{21} & \sigma_{22} \end{bmatrix}$,

$$\sigma_{ii} = 1 - (|S_{ii}|^2 - |S_{ij}|^2), \quad \text{and}$$
$$\sigma_{ij} = -(S_{ii}^* S_{ij} + S_{ji} S_{jj}^*)$$

Figure 36.C depicts the measured and simulated CCL of the proposed system. We found that CCL over the entire operational bandwidth was less than 0.1 bps/Hz.

V. COMPARISON WITH STATE-OF-THE-ART WORK

Table. 4 summarizes the full comparison of the proposed and recent published mm-wave MIMO antennas. It can be inferred that when the proposed antenna is compared to [10], [21], [32], [33], and [34], it has the best isolation, gain, impedance bandwidth, and ECC values. In contrast, [11], [18], [23], [29], and [36] reported greater gain and impedance bandwidth values than our suggested antenna, but with a lower ECC and CCL. The presented antenna design demonstrates superior MIMO performance to that of the other antennas discussed above. Despite the large size of this antenna, it is perfectly suitable for the proposed application, which is device-to-device (D2D) communication in smart cities such as cars, automobiles, and smart devices in smart homes.

VI. CONCLUSION

It is presented in this paper how to apply the TCM to the design of a multi-antenna system for 5G wireless communication systems in a systematic manner. Therefore, in this article, this theory was applied to the novel design of a

2-port MIMO logarithmic spiral patch antenna in order to systematically place the antenna ports with low correlation. The systematic design method was implemented with the idea of starting with a single element that has a single logarithmic spiral arm, moving through an array that has two logarithmic spiral arms, and coming to a conclusion with four configurations, including 2-port MIMO and the best performance out of those four. The four different 2-port MIMO configurations, namely face-to-face, side by side, oppositely side by side, and orthogonal 2-port MIMO logarithmic spiral patch antennas, are designed and analyzed using characteristic mode analysis to select the best one in performance. There is a high correlation between experimental and simulated outcomes. Because of its considerable return loss, wide bandwidth, high gain, low ECC, low CCL, and strong element isolation characteristics, the suggested oppositely side by side 2-port MIMO antenna could be a good choice for 5G wireless communication systems.

REFERENCES

[1] T. S. Rappaport, S. Sun, R. Mayzus, H. Zhao, Y. Azar, K. Wang, G. N. Wong, J. K. Schulz, M. Samimi, and F. Gutierrez, "Millimeter wave mobile communications for 5G cellular: It will work!" *IEEE Access*, vol. 1, pp. 335–349, 2013.

[2] J. G. Andrews, S. Buzzi, W. Choi, S. V. Hanly, A. Lozano, A. C. K. Soong, and J. C. Zhang, "What will 5G be?" *IEEE J. Sel. Areas Commun.*, vol. 32, no. 6, pp. 1065–1082, Jun. 2014.

[3] Z. Pi and F. Khan, "An introduction to millimeter-wave mobile broadband systems," *IEEE Commun. Mag.*, vol. 49, no. 6, pp. 101–107, Jun. 2011.

[4] J. Thompson, X. Ge, H.-C. Wu, R. Irmer, H. Jiang, G. Fettweis, and S. Alamouti, "5G wireless communication systems: Prospects and challenges [guest editorial]," *IEEE Commun. Mag.*, vol. 52, no. 2, pp. 62–64, Feb. 2014.

[5] A. Ghosh, A. Maeder, M. Baker, and D. Chandramouli, "5G evolution: A view on 5G cellular technology beyond 3GPP release 15," *IEEE Access*, vol. 7, pp. 127639–127651, 2019.

[6] J. Zhang, X. Ge, Q. Li, M. Guizani, and Y. Zhang, "5G millimeter-wave antenna array: Design and challenges," *IEEE Wireless Commun.*, vol. 24, no. 2, pp. 106–112, Apr. 2017.

[7] I. Shayea, T. A. Rahman, M. H. Azmi, and M. R. Islam, "Real measurement study for rain rate and rain attenuation conducted over 26 GHz microwave 5G link system in Malaysia," *IEEE Access*, vol. 6, pp. 19044–19064, 2018.

[8] S. Y. A. Fat, E. K. I. Hamad, W. Swelam, A. M. Allam, and H. A. E. Mohamed, "Design of compact 4-Port MIMO antenna based on Minkowski fractal shape DGS for 5G applications," *Prog. Electromagn. Res. C*, vol. 113, pp. 123–136, Jun. 2021.

[9] A. Abdelaziz and E. K. I. Hamad, "Isolation enhancement of 5G multiple-input multiple-output microstrip patch antenna using metamaterials and the theory of characteristic modes," *Int. J. RF Microw. Comput.-Aided Eng.*, vol. 30, no. 11, Nov. 2020, Art. no. e22416.

[10] Y. Zhang, J.-Y. Deng, M.-J. Li, D. Sun, and L.-X. Guo, "A MIMO dielectric resonator antenna with improved isolation for 5G mm-Wave applications," *IEEE Antennas Wireless Propag. Lett.*, vol. 18, no. 4, pp. 747–751, Apr. 2019.

[11] M. Khalid, S. I. Naqvi, N. Hussain, M. Rahman, S. S. Mirjavadi, M. J. Khan, and Y. Amin, "4-Port MIMO antenna with defected ground structure for 5G millimeter wave applications," *Electronics*, vol. 9, no. 1, pp. 1–7, 2020.

[12] A. Ghalib and M. S. Sharawi, "TCM analysis of defected ground structures for MIMO antenna designs in mobile terminals," *IEEE Access*, vol. 5, pp. 19680–19692, 2017.

[13] E. K. I. Hamad and A. Abdelaziz, "Performance of a metamaterial-based 1×2 microstrip patch antenna array for wireless communications examined by characteristic mode analysis," *Radioengineering*, vol. 28, no. 4, pp. 681–689, 2019.

[14] N. Rao and V. D. Kumar, "Gain and bandwidth enhancement of a microstrip antenna using partial substrate removal in multiple-layer dielectric substrate," in *Proc. Prog. Electromagn. Res. Symp.*, Suzhou, China, 2011, pp. 1285–1289.

[15] W. A. E. Ali, H. A. Mohamed, A. A. Ibrahim, and M. Z. M. Hamdalla, "Gain improvement of tunable band-notched UWB antenna using metamaterial lens for high speed wireless communications," *Microsyst. Technol.*, vol. 25, no. 11, pp. 4111–4117, Nov. 2019.

[16] X. Zhang, Y. Han, W. Li, and X. Duan, "A rectangular planar spiral antenna for GIS partial discharge detection," *Int. J. Antennas Propag.*, vol. 2014, pp. 1–7, May 2014.

[17] K. K. Naik, "Design of spiral square patch antenna for wireless communications," in *Contemporary Developments in High-Frequency Photonic Devices*. Hershey, PA, USA: IGI Global, 2019, pp. 131–141.

[18] N. Hussain, M.-J. Jeong, A. Abbas, and N. Kim, "Metasurface-based single-layer wideband circularly polarized MIMO antenna for 5G millimeter-wave systems," *IEEE Access*, vol. 8, pp. 130293–130304, 2020.

[19] D. A. Sehrai, M. Abdullah, A. Altaf, S. H. Kiani, F. Muhammad, M. Tufail, M. Irfan, A. Glowacz, and S. Rahman, "A novel high gain wideband MIMO antenna for 5G millimeter wave applications," *Electronics*, vol. 9, no. 6, p. 1031, Jun. 2020.

[20] N. Shoaib, S. Shoaib, R. Y. Khattak, I. Shoaib, X. Chen, and A. Perwaiz, "MIMO antennas for smart 5G devices," *IEEE Access*, vol. 6, pp. 77014–77021, 2018.

[21] A. Iqbal, A. Basir, A. Smida, N. K. Mallat, I. Elfergani, J. Rodriguez, and S. Kim, "Electromagnetic bandgap backed millimeter-wave MIMO antenna for wearable applications," *IEEE Access*, vol. 7, pp. 111135–111144, 2019.

[22] J. S. Park, J.-B. Ko, H.-K. Kwon, B.-S. Kang, B. Park, and D. Kim, "A tilted combined beam antenna for 5G communications using a 28-GHz band," *IEEE Antennas Wireless Propog. Lett.*, vol. 15, pp. 1685–1688, 2016.

[23] S. F. Jilani and A. Alomainy, "Millimetre-wave T-shaped MIMO antenna with defected ground structures for 5G cellular networks," *IET Microw., Antennas Propag.*, vol. 12, no. 5, pp. 672–677, Apr. 2018.

[24] N. Hussain, M.-J. Jeong, J. Park, and N. Kim, "A broadband circularly polarized Fabry–Perot resonant antenna using a single-layered PRS for 5G MIMO applications," *IEEE Access*, vol. 7, pp. 42897–42907, 2019.

[25] R. J. Garbacz and R. Turpin, "A generalized expansion for radiated and scattered fields," *IEEE Trans. Antennas Propag.*, vol. AP-19, no. 3, pp. 348–358, May 1971.

[26] R. F. Harrington and J. R. Mautz, "Theory of characteristic modes for conducting bodies," *IEEE Trans. Antennas Propag.*, vol. AP-19, no. 5, pp. 622–628, Sep. 1971.

[27] R. F. Harrington and J. R. Mautz, "Computation of characteristic modes for conducting bodies," *IEEE Trans. Antennas Propag.*, vol. AP-19, no. 5, pp. 629–639, Sep. 1971.

[28] M. Cabedo-Fabres, E. Antonino-Daviu, A. Valero-Nogueira, and M. F. Bataller, "The theory of characteristic modes revisited: A contribution to the design of antennas for modern applications," *IEEE Antennas Propag. Mag.*, vol. 49, no. 5, pp. 52–68, Oct. 2007.

[29] S.-X. Ta and I. Park, "Low-profile broadband circularly polarized patch antenna using metasurface," *IEEE Trans. Antennas Propag.*, vol. 63, no. 12, pp. 5929–5934, Dec. 2015.

[30] S. Blanch, J. Romeu, and I. Corbella, "Exact representation of antenna system diversity performance from input parameter description," *Electron. Lett.*, vol. 39, no. 9, pp. 705–707, May 2003.

[31] M. Akbari, H. A. Ghalyon, M. Farahani, A.-R. Sebak, and T. A. Denidni, "Spatially decoupling of CP antennas based on FSS for 30-GHz MIMO systems," *IEEE Access*, vol. 5, pp. 6527–6537, 2017.

[32] Z. Wani, M. P. Abegaonkar, and S. K. Koul, "A 28-GHz antenna for 5G MIMO applications," *Prog. Electromagn. Res. Lett.*, vol. 78, pp. 73–79, Aug. 2018.

[33] W. Ali, S. Das, H. Medkour, and S. Lakrit, "Planar dual-band 27/39 GHz millimeter-wave MIMO antenna for 5G applications," *Microsyst. Technol.*, vol. 27, no. 1, pp. 283–292, Jan. 2021.

[34] K. Raheel, A. Altaf, A. Waheed, S. H. Kiani, D. A. Sehrai, F. Tubbal, and R. Raad, "E-shaped H-slotted dual band mmWave antenna for 5G technology," *Electronics*, vol. 10, no. 9, pp. 10–19, 2021.

[35] M. M. Kamal, S. Yang, X.-C. Ren, A. Altaf, S. H. Kiani, M. R. Anjum, A. Iqbal, M. Asif, and S. I. Saeed, "Infinity shell shaped MIMO antenna array for mm-wave 5G applications," *Electronics*, vol. 10, no. 2, pp. 1–10, 2021.

[36] S.-J. Park, D.-H. Shin, and S.-O. Park, "Low side-lobe substrate-integrated-waveguide antenna array using broadband unequal feeding network for millimeter-wave handset device," *IEEE Trans. Antennas Propag.*, vol. 64, no. 3, pp. 923–932, Mar. 2015.

AHMED ABDELAZIZ was born in Aswan, Egypt, in 1992. He received the B.E. degree in electronic and communication engineering from the Arab Academy for Science, Technology and Maritime Transport, Egypt, in 2014, the master's degree in electrical engineering from the Faculty of Engineering, Aswan University, Aswan, in February 2019, where he is currently pursuing the Ph.D. degree in designing and optimizing MIMO antenna systems for 5G wireless communications. His master's thesis was entitled Design of Microstrip Antennas Using Metamaterials and Characteristics Mode Theory for 5G Wireless Communications. He is also working as a Teaching/a Research Assistant with the Department of Electronics and Communications, Luxor Higher Institute of Engineering and Technology, Luxor, Egypt. His current research interests include the antenna design, metamaterials, characteristic mode theory, and 5G.

HESHAM A. MOHAMED (Senior Member, IEEE) received the B.Sc. degree in electronics and communication engineering from the University of Menofia, in 2003, and the M.Sc. and Ph.D. degrees from Ain Shams University, in 2009 and 2014, respectively. He is currently an Associate Professor with Electronics Research Institute (ERI), Giza, Egypt. He has teaching experience (more than 12 years of experience) as a Lecturer with the Electronic and Communication Engineering Department, Faculty of Engineering, Misr University for Science and Technology. He has authored or coauthored close to 30 journal articles and about 17 refereed conference papers, and attended and chaired several national and international conferences. He has supervised and co-supervised four Ph.D. and four M.Sc. theses at Cairo University, Ain shams University, Benha University, and Helwan University, the outstanding publications of his work in ranked international journals and conferences. He participates in more than six research projects at the national and international levels as the Egypt-NSF-USA Joint Fund Program, the Egypt STDF-France IRD Joint Fund Program, and the European Committee programs of FP6 and FP7. His role is from C-PI to PI. He was an RF-Design Engineer (antenna and power amplifier module) in the project "Small SAR Satellite Antenna and Transceiver System" (2018–2020), a Communication Subsystem Engineer in the project "Egyptian University Satellite (EUS-2)" (2019–2020), an RF-Design Engineer in the project "Design of Radar Absorbing Materials (RAM) Using Meta-materials" (2018–2019), a Wireless System Engineer in the project "Development of High Data Rate X-Band Transmitter for LEO Remote Sensing Satellites" (2015–2018), an RF-Design Engineer in the project "THE EGYPTION 2D RADAR" (2015–2018), an RF Design Engineer in the project "Ultra-Wideband Ground Penetrating Radar for Water Detection in Egypt" (2011–2014), and an RF-Design Engineer in the project "Novel Planar Antennas for the Most Recent Telecommunications Applications" (February 2011–February 2014). His research interests include microwave circuit designs, planar antenna systems, recently on EBG structures, UWB components and antenna and RFID systems, radar absorbing materials, energy harvesting and wireless power transfer, smart antennas, microstrip antennas, microwave filters, metamaterials, and MIMO antennas and its applications in wireless communications. He is a Reviewer of the international journals, including IEEE Microwave and Wireless Components Letters, IEEE Access, *Progress in Electromagnetics Research* (*PIER*, *PIER B*, *PIER C*, *PIER M*, and *PIER Letters*), *Microwave and Optical Technology Letters*, and the *International Journal of Circuit Theory and Applications*.

EHAB K. I. HAMAD (Member, IEEE) received the B.Sc. and M.Sc. degrees in electrical engineering from Assiut University, Egypt, in 1994 and 1999, respectively, and the Ph.D. degree in electrical engineering from Otto von Guericke Magdeburg University, Magdeburg, Germany, in 2006.

From 1996 to 2001, he was a Teaching/a Research Assistant with the Aswan Faculty of Engineering, South Valley University. From July 2001 to December 2006, he was a Research Assistant with the Chair of Microwave and Communication Engineering, Otto-von-Guericke University Magdeburg. From July 2010 to April 2011, he was with the School of Computing and Engineering, University of Huddersfield, Huddersfield, U.K., as a Postdoctoral Research Assistant. He is currently a Full Professor for antenna engineering with the Department of Electrical Engineering, Faculty of Engineering, Aswan University, Aswan, Egypt. He has authored or coauthored over 60 technical peer-reviewed papers in international journals and conference proceedings. His current research interests include antenna design, microstrip antennas, MIMO antennas, mm-wave antennas, multi-band/wide-band small antennas for 4G/5G, metamaterials, metasurfaces, UWB, RFID, RF energy harvesting, and implanted antennas for bio-medical applications. He is also interested in designing microstrip antennas using the theory of characteristic modes and designing antennas in the THz frequency band using graphene plasmonic material.

Dr. Hamad has been a member of the Middle East Organization of Microwave, Antennas, and Propagation (MEOMAP) since March 2019 and the Engineering Syndicate, Egypt, since 1994. He received a best paper award. He is also a Reviewer of many journals, including IEEE Transactions on Antennas and Propagation, *IET Microwaves, Antennas and Propagation*, *Electronics Letters*, *Radioengineering*, *PIERs*, the *Journal of Electrical Engineering*, the journal of *Recent Advances in Electrical and Electronic Engineering*, and *Microwave and Optical Technology Letters*, and many international conferences, including EuCAP, National Radio Sciences, and Asia-Pacific Microwave Conference, and some others on Easy Chair and EDAS.